crystals

MDPI

Article

Investigating the Formation of Different $(NH_4)_2[M(H_2O)_5(NH_3CH_2CH_2COO)]_2[V_{10}O_{28}]\cdot nH_2O$ (M = Co^{II}, Ni^{II}, Zn^{II}, n = 4; M = Cd^{II}, Mn^{II}, n = 2) Crystallohydrates

Jana Chrappová [1,*], Yogeswara Rao Pateda [1,*], Lenka Bartošová [2] and Erik Rakovský [1]

[1] Department of Inorganic Chemistry, Faculty of Natural Sciences, Comenius University in Bratislava, Ilkovičova 6, 842 15 Bratislava, Slovakia; erik.rakovsky@uniba.sk
[2] Department of Food Databases, Food Research Institute, National Agricultural and Food Centre, Priemyselná 4, 824 75 Bratislava, Slovakia; lenka.bartosova@nppc.sk
* Correspondence: jana.chrappova@uniba.sk (J.C.); rao2@uniba.sk (Y.R.P.)

Abstract: Three hybrid compounds based on decavanadates, i.e., $(NH_4)_2[Co(H_2O)_5(\beta\text{-HAla})]_2[V_{10}O_{28}]\cdot 4H_2O$ (**1**), $(NH_4)_2[Ni(H_2O)_5(\beta\text{-HAla})]_2[V_{10}O_{28}]\cdot 4H_2O$ (**2**), and $(NH_4)_2[Cd(H_2O)_5(\beta\text{-HAla})]_2[V_{10}O_{28}]\cdot 2H_2O$ (**3**), (where β-Hala = zwitterionic form of β-alanine) were prepared by reactions in mildly acidic conditions (pH ~ 4) at room temperature. These compounds crystallise in two structure types, both crystallising in monoclinic $P2_1/n$ space group but with dissimilar cell packing, i.e., as tetrahydrates (**1** and **2**) and as a dihydrate (**3**). An influence of crystal radii and spin state of the central atom in $[M(H_2O)_5(\beta\text{-HAla})]^{2+}$ complex cations on the crystal packing leading to the formation of different crystallohydrate forms was investigated together with previously prepared $(NH_4)_2[Zn(H_2O)_5(\beta\text{-HAla})]_2[V_{10}O_{28}]\cdot 4H_2O$ (**4**) and $(NH_4)_2[Mn(H_2O)_5(\beta\text{-HAla})]_2[V_{10}O_{28}]\cdot 2H_2O$ (**5**) and spin states of $[M(H_2O)_5(\beta\text{-HAla})]^{2+}$ (M = Co^{2+}, Ni^{2+}, and Mn^{2+}) cations in solution were confirmed by ^{1}H-NMR paramagnetic effects. FT-IR and FT-Raman spectra for **1**–**5** are in agreement with the X-ray structure analysis results.

Keywords: hybrid decavanadates; β-alanine; crystallohydrates; crystal structure; vibrational spectroscopy; paramagnetic NMR

check for updates

Citation: Chrappová, J.; Pateda, Y.R.; Bartošová, L.; Rakovský, E. Investigating the Formation of Different $(NH_4)_2[M(H_2O)_5(NH_3CH_2CH_2COO)]_2[V_{10}O_{28}]\cdot nH_2O$ (M = Co^{II}, Ni^{II}, Zn^{II}, n = 4; M = Cd^{II}, Mn^{II}, n = 2) Crystallohydrates. *Crystals* **2024**, *14*, 685. https://doi.org/10.3390/cryst14080685

Academic Editor: Pedro Marques De Almeida

Received: 4 July 2024
Revised: 23 July 2024
Accepted: 24 July 2024
Published: 27 July 2024

Copyright: © 2024 by the authors. Licensee MDPI, Basel, Switzerland. This article is an open access article distributed under the terms and conditions of the Creative Commons Attribution (CC BY) license (https://creativecommons.org/licenses/by/4.0/).

1. Introduction

Decavanadate anion is the predominant and most stable V(V) oxo-anion found in the acidic aqueous solutions [1]. It is known in different protonation states, $[H_nV_{10}O_{28}]^{(6-n)-}$ (n = 0–4) [2–4].

The decavanadate anion consists of ten edge-sharing VO_6 octahedra. Six of them form a rectangular 2 × 3 arrangement, with two VO_6 octahedra joining the arrangement from the top and two from the bottom via edge sharing with the six octahedra lying in the central plane. The ideal symmetry of $[V_{10}O_{28}]^{6-}$ anion is given by the D_{2h} point group symmetry. In most crystal structures, $[V_{10}O_{28}]^{6-}$ anion usually occupies special positions, mostly inversion centres, and its symmetry is changed correspondingly; however, its geometry remains close to the ideal D_{2h} symmetry.

In crystal structures, decavanadates act as acceptors of protons in supramolecular arrangements; protonated decavanadate species can also act as proton donors. Typically, if decavanadate anion is not protonated on mutually centrosymmetrically arranged sites, such decavanadate anions will likely form a centrosymmetric dimer interconnected via anion-anion hydrogen bonds [5] or via hydrogen bonding to counter-cations lying on a centre of symmetry [6]. Considering the sterical effect of the decavanadate anion and the influence of size, shape, and nature of counter-cations, a substantial part of decavanadates include water molecules as a stabilising element of the crystal structure. Formation of different crystallohydrates depends on reaction conditions [7] or on temperature changes,

even if the reaction conditions remain the same [8]. As a result, decavanadates are known to form a large variety of supramolecular assemblies [9].

The oxovanadates (V), including decavanadates and peroxovanadium compounds, are of great interest in bioinorganic chemistry and biochemistry because of their antidiabetic, antibacterial, antiprotozoal, antiviral, and anticancer properties [10,11]. Studying of non-covalent interactions based on electrostatic attractive forces between decavanadate anion and appropriate molecules (organic cations, hybrid inorganic–organic complex cations, and biomacromolecules) could provide important information on the cooperative effects of decavanadate ions in biological systems [12–14].

Apart from the biological importance of decavanadates, there are other emerging application possibilities. Some decavanadates exhibit water oxidation activity [15] or heterogeneous bifunctional catalytic properties in the selective oxidation of sulphides and Mannich reaction [16]. Decavanadates with superior proton conductivity [17] and photoluminescent sensing properties for the detection of Zn^{2+} and Co^{2+} [18] were also prepared. Ammonium decavanadate nanodots—holey reduced graphene oxide nanoribbons [19] and α-$Co(OH)_2$ nanoplates with decavanadate anion [20] can be used as electrodes for supercapacitors.

In this work, we report the synthesis, crystal structure determination, and properties of three decavanadates, i.e., $(NH_4)_2[Co(H_2O)_5(\beta\text{-HAla})]_2[V_{10}O_{28}]\cdot 4H_2O$ (**1**), $(NH_4)_2[Ni(H_2O)_5(\beta\text{-HAla})]_2[V_{10}O_{28}]\cdot 4H_2O$ (**2**), and $(NH_4)_2[Cd(H_2O)_5(\beta\text{-HAla})]_2[V_{10}O_{28}]\cdot 2H_2O$ (**3**), prepared by the same procedure we used previously for the preparation of two decavanadates containing the same $[M(H_2O)_5(\beta\text{-HAla})]^{2+}$ cations in two different crystallohydrate forms, i.e., tetrahydrate $(NH_4)_2[Zn(H_2O)_5(\beta\text{-HAla})]_2[V_{10}O_{28}]\cdot 4H_2O$ (**4**) and dihydrate $(NH_4)_2[Mn(H_2O)_5(\beta\text{-HAla})]_2[V_{10}O_{28}]\cdot 2H_2O$ (**5**) [21]. The compounds **1** and **2** are isostructural with **4**, while **3** is isostructural with **5**. In [22], compound **2** was prepared by using an alternative hydrothermal "Direct Synthesis" approach by the reaction of metal powder in anion-deficient conditions with V_2O_5 in an aqueous solution of β-alanine and ammonium acetate. Subsequently, compound **2** was used as a precursor for the preparation of V_2O_5/MnV_2O_6 mixed oxide, and its ability to act as a water oxidation catalyst for oxygen production was studied. Later, **1** was prepared by the same "Direct Synthesis" method and used as a precursor for the preparation of solid mixed oxides CoV_2O_6/V_2O_5 and $Co_2V_2O_7/V_2O_5$ by thermal decomposition; both these mixed oxides and **1** can act as catalysts for photoinduced water oxidation [23]. The aim of the present study is to obtain more complete insight into the formation of different crystallohydrates with the general formula $(NH_4)_2[M(H_2O)_5(\beta\text{-HAla})]_2[V_{10}O_{28}]\cdot nH_2O$, where *M* is a divalent metal ion, from the same reaction conditions.

2. Materials and Methods

2.1. General

All chemicals were of reagent or better grade, obtained from commercial sources (Mikrochem (Pezinok, Slovakia), Sigma-Aldrich (Saint Louis, MI, USA), Slavus (Donja Stubica, Croatia), Lachema (Brno, Czech Republic)). Infrared spectra were obtained from KBr pellets on a Thermo Scientific Nicolet 6700 FTIR spectrometer in the 400–4000 cm^{-1} range (Waltham, MA, USA). The Raman spectra were registered with a Raman microspectrometer Senterra (Bruker Optik, Ettlingen, Germany), using a laser with the wavelength 532 nm, with a maximum power of 2 mW, in the range 64–4467 cm^{-1}, with 10× objective lenses, and 2 scans for 10 s each. ^{1}H-NMR spectra were recorded on a Bruker AVANCE Neo 400 MHz (operating at 9.37 T, 400 MHz) using D_2O as a reference. Chemical shifts are reported in Hz. Vanadium (V) was determined volumetrically by titration with $FeSO_4$ (c = 0.1 M) using diphenylamine as the indicator.

2.2. Synthesis and Crystallisation

2.2.1. Synthesis of $(NH_4)_2[Co(H_2O)_5(\beta\text{-HAla})]_2[V_{10}O_{28}]\cdot 4H_2O$ (**1**)

$CoSO_4.7H_2O$ (1.4055 g; 5 mmol) was added to a solution of β-alanine (0.89 g; 10 mmol) in water (20 mL). After stirring for 15 min, a solution of NH_4VO_3 (1.170 g; 10 mmol) in water (40 mL) was added under the immediate formation of a fine precipitate. The solution with precipitate was stirred for 30 min and filtered. The pH of the filtrate was adjusted to 4.0 with 2M H_2SO_4. To the reddish-brown solution obtained, ethanol (10 mL) was added. Reddish brown crystals were isolated after standing for 22 days at 4 °C in the refrigerator.

Yield: 0.8 g/52.1% (calc. for vanadium). Anal. Calc. for $C_6H_{50}N_4O_{46}Co_2V_{10}$ (MW = 1541.76 g/mol) V, 34.10%. Found: V, 33.96%.

2.2.2. Synthesis of $(NH_4)_2[Ni(H_2O)_5(\beta\text{-HAla})]_2[V_{10}O_{28}]\cdot 4H_2O$ (**2**)

$NiCl_2.6H_2O$ (1.188 g; 5 mmol) was added to a solution of β-alanine (0.89 g; 10 mmol) in water (20 mL). After stirring for 15 min, a solution of NH_4VO_3 (1.170 g; 10 mmol) in water (60 mL) was added, followed by the immediate formation of a fine precipitate. The solution with precipitate was stirred for 30 min and filtered. The pH of the filtrate was adjusted to 4.0 with 4M HCl. To the yellow solution obtained, ethanol (10 mL) was added. Dark orange crystals with an intense green tone were isolated after standing for 20 days at 4 °C in the refrigerator.

Yield: 1.343 g/87.5% (calc. for vanadium). Anal. Calc. for $C_6H_{50}N_4O_{46}Ni_2V_{10}$ (MW = 1541.32 g/mol) V, 34.11%. Found: V, 33.69%.

2.2.3. Synthesis of $(NH_4)_2[Cd(H_2O)_5(\beta\text{-HAla})]_2[V_{10}O_{28}]\cdot 2H_2O$ (**3**)

$Cd(NO_3)_2.4H_2O$ (1.542 g; 5 mmol) was added to a solution of β-alanine (0.89 g; 10 mmol) in water (20 mL). After stirring for 15 min, a solution of NH_4VO_3 (1.170 g; 10 mmol) in water (40 mL) was added, followed by the immediate formation of a fine precipitate. The solution with precipitate was stirred for 30 min and filtered. The pH of the filtrate was adjusted to 4.25 with 4M HNO_3. To the yellow solution obtained, ethanol (10 mL) was added. Orange crystals were isolated after standing for 15 days at 4 °C in the refrigerator.

Yield: 0.702 g/43.7% (calc. for vanadium). Anal. Calc. for $C_6H_{46}N_4O_{44}Cd_2V_{10}$ (MW = 1612.67 g/mol) V, 31.59%. Found: V, 31.44%.

$(NH_4)_2[Zn(H_2O)_5(\beta\text{-HAla})]_2[V_{10}O_{28}]\cdot 4H_2O$ (**4**) and $(NH_4)_2[Mn(H_2O)_5(\beta\text{-HAla})]_2[V_{10}O_{28}]\cdot 2H_2O$ (**5**) samples were prepared for physical measurements according to [22].

2.3. X-ray Data Collection and Structure Determination

Intensity data for the compounds **1**–**3** were collected on a Kuma KM–4 CCD diffractometer using graphite monochromated MoKα radiation (0.71073 Å) by the ω- and φ-scan techniques at room temperature. Data collection, data reduction, and finalisation were carried out using *CrysAlis Pro-Version 1.171.43.128a* software [24]. Intensity data for **4** and **5** were reprocessed from original images collected under the conditions in [21] by using the above-mentioned up-to-date version of *CrysAlis Pro* software to take advantage of improved data processing, especially regarding twin data reduction handling.

The structures were solved by *SHELXT* [25] and refined by the full matrix least-squares method on all F^2 data using *SHELXL-2018/3* [26]. All non-hydrogen atoms were refined anisotropically. Hydrogen atoms of methylene groups were refined using a riding model, and the ammonium group was refined as a free rotor, with C–H and N–H distances free to refine. Hydrogen atoms of water molecules were refined with all O–H and all H. . .H distances restrained to be equal; similarly, the tetrahedral shape of ammonium cation was retained by restraining all N–H and all H. . .H distances to be equal. Thermal parameters of the H atoms were constrained to $U_{iso}(H) = 1.2U_{eq}(C)$ and $U_{iso}(H) = 1.5U_{eq}(N, O)$.

Both compounds **3** and **5** crystallise as non-merohedral twins. Two domains related to the twofold rotation about the *c*-axis were found using *Ewald Explorer* in the *CrysAlis Pro*

software, and data were refinalised using internal programme features. The twin domain volume ratios were refined to 0.6515(7):0.3485(7) for **3** and 0.8436(4):0.1564(4) for **5**.

Geometrical calculations were performed using *SHELXL-2018/3*, *Olex2 1.5* [27], and *PARST* [28]. *Olex2 1.5* and *DIAMOND* [29] were used for molecular graphics. Octahedral distortion parameters ζ [30], Δ [31], Σ [32], and Θ [33] were calculated using *OctaDist 3.1.0* [34]. Hydrogen bonding geometries were normalised to neutron distances following a literature procedure [35,36].

Crystal data, conditions of data collection, and refinement results for the compounds **1**–**5** are reported in Table S1.

2.4. Paramagnetic ^{1}H-NMR Measurements

For the Evans method [37–39], approx. 2 mM solutions of **1**, **2**, **4**, and **5** using 3% (v/v) *t-Bu*OH solution in H_2O were prepared. The inner n.m.r. tube (o.d. 2 mm) was loaded with 3% (v/v) *t-Bu*OH solution in D_2O as a reference. The outer n.m.r. tube (o.d. 5 mm) was filled with 500 µL of the sample solution.

The Δf value, defined as the difference between the chemical shift of the ^{1}H-NMR *t-Bu* signal in the sample solution and that of the *t-Bu*OH reference solution, was used to calculate the molar susceptibility of the complex using the following equation:

$$\chi_{\mathrm{m}} = \frac{3\Delta f}{4\pi c f} \quad (1)$$

where c is the concentration of the paramagnetic complex in the solution in mmol.L^{-1} and f is the spectrometer frequency (400 MHz). Considering there are 2 $[M(H_2O)_5(\beta\text{-HAla})]^{2+}$ cations per formula unit, the value of c is twice the concentration of the compound in the solution.

The χ_{p} values [cm^{3}mol^{-1}] are molar susceptibilities corrected for diamagnetic contribution to the susceptibility in the sample.

$$\chi_{\mathrm{p}} = \chi_{\mathrm{m}} - \chi_{\mathrm{d}} \quad (2)$$

where χ_{d} represents diamagnetic contributions from the ligands, ions, inner-core electrons, etc. [40]. The following values were used to calculate the effective magnetic moment:

$$\mu_{eff} = \sqrt{\frac{3kT\chi_{\mathrm{p}}}{N_{\mathrm{A}}\mu_{\mathrm{B}}^2}} \quad (3)$$

where k is the Boltzmann constant, T is temperature [K], N_{A} is Avogadro's number, and μ_{B} is the Bohr magneton. Effective magnetic moment is compared to the calculated value for the central atom in question as follows [41]:

$$\mu_{cal} = 2\sqrt{S(S+1)}\mu_{\mathrm{B}} \quad (4)$$

3. Results and Discussion

Decavanadates with complex cations, i.e., $(NH_4)_2[Co(H_2O)_5(\beta\text{-HAla})]_2[V_{10}O_{28}]\cdot 4H_2O$ (**1**), $(NH_4)_2[Ni(H_2O)_5(\beta\text{-HAla})]_2[V_{10}O_{28}]\cdot 4H_2O$ (**2**), and $(NH_4)_2[Cd(H_2O)_5(\beta\text{-HAla})]_2[V_{10}O_{28}]\cdot 2H_2O$ (**3**), were obtained by crystallisation from the β-alanine—$CoSO_4$—NH_4VO_3—H_2SO_4—H_2O—ethanol (**1**), β-alanine—$NiCl_2$—NH_4VO_3—HCl—H_2O—ethanol (**2**), and β-alanine—$Cd(NO_3)_2$—NH_4VO_3—HNO_3—H_2O—ethanol (**3**) reaction systems in mildly acidic (pH~4) conditions. Attempts to prepare compounds of Mg^{2+}, Sr^{2+}, Ba^{2+}, Pb^{2+}, and Hg^{2+} from the same reaction system were unsuccessful, obtaining ammonium decavanadate as a product.

The preparation of compound **1** by the hydrothermal reaction of cobalt powder with V_2O_5 in an aqueous solution containing β-alanine and ammonium acetate was reported earlier [23]. However, from the described green colour of the solution and products obtained

by hydrothermal synthesis when compared with the orange product we obtained, it can be inferred that a partial reduction of V(V) to V(IV) has taken place. This partial reduction can be avoided by using our preparation method. Although the synthesis was targeted towards using the prepared compound as a precursor for the preparation of mixed Co/V oxides by thermal decomposition, to avoid the presence of lower oxidation states of vanadium in the products, not only during the reactions in solutions but even after thermal decomposition in the air atmosphere, it is a good practise to use purified V(V) precursors [42].

3.1. Crystallographic Characterisation of Prepared Compounds

All prepared compounds belong to one of two monoclinic (space group $P2_1/n$) structure types with substantially different cell parameters and cell packing—tetrahydrates (**1**, **2,** and **4**) (Figure 1a) and dihydrates (**3** and **5**) (Figure 1b).

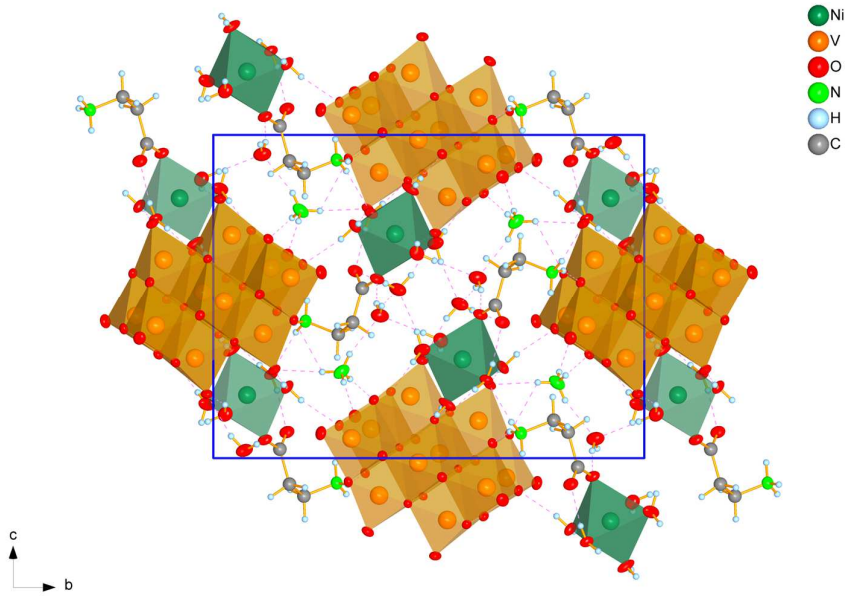

(**a**)

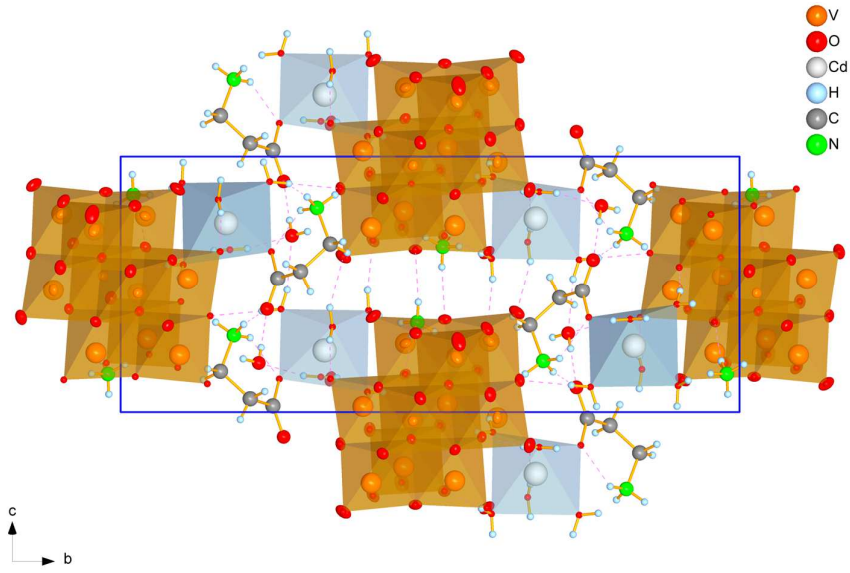

(**b**)

Figure 1. A view of the cell packing of tetrahydrates (**2** as an example) (**a**) and dihydrates (**3** as an example) (**b**) along the *a*-axis. Dashed lines indicate hydrogen bonds, blue rectangle denote unit cell boundaries.

The asymmetric unit of all prepared dihydrates consists of one half of the $[V_{10}O_{28}]^{6-}$ anion with C_i symmetry lying on an inversion centre, one $[M(H_2O)_5(\beta\text{-HAla})]^{2+}$ cation, one NH_4^+ cation, and two water molecules in general positions (Figure 2a).

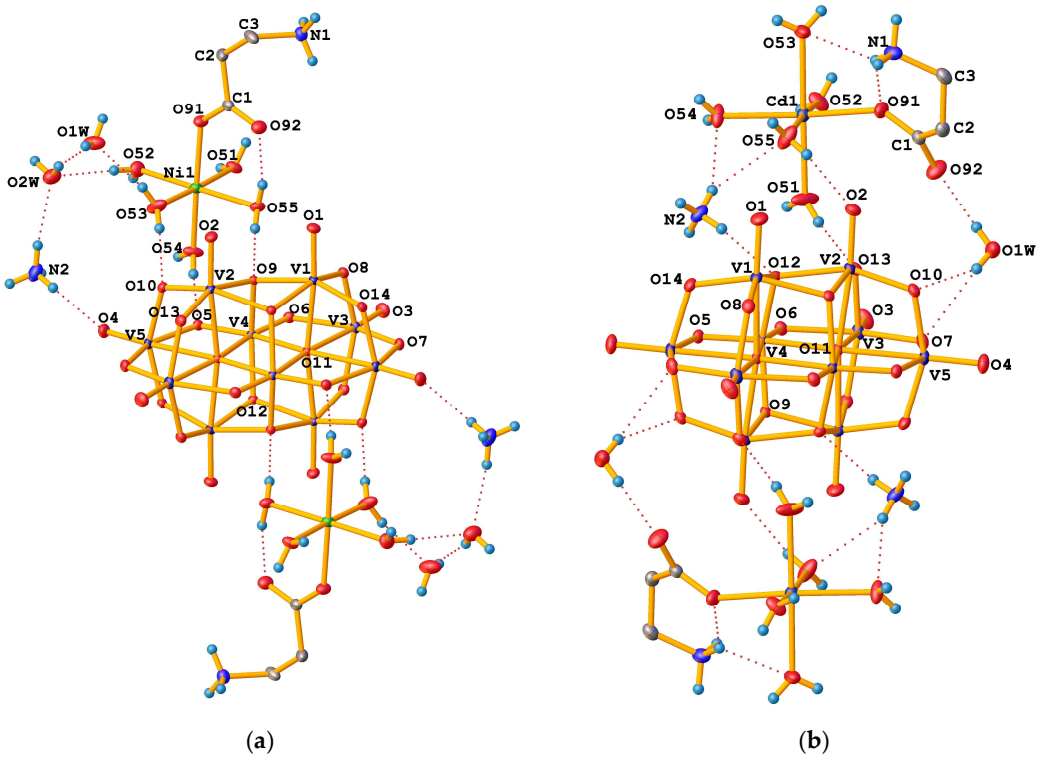

Figure 2. ADP representations of the crystal structure of (**a**) tetrahydrates (**2** as an example) and (**b**) dihydrates (**3** as an example) with numbering scheme (methylene H atoms are excluded). Labelled atoms are related to the unlabelled ones by the centre of symmetry. Displacement ellipsoids are drawn at 30% probability level. Dashed lines indicate hydrogen bonds.

The asymmetric unit of tetrahydrates consists of one half of the $[V_{10}O_{28}]^{6-}$ anion with C_i symmetry lying on an inversion centre, one $[M(H_2O)_5(\beta\text{-HAla})]^{2+}$ cation, one NH_4^+ cation, and one water molecule in general positions (Figure 2b).

The quality of X-ray diffraction data allowed us to find all hydrogen atoms from the ifference electron density map and refine them semi-freely using a set of suitable restraints [43]. As a result, the accurate orientations of water molecules, $-NH_3^+$ groups, and NH_4^+ cations were successfully determined.

The following four types of oxygen atoms can be distinguished in the decavanadate anions: terminal O_T bonded to only one vanadium atom, and $O(\mu_2)$, $O(\mu_3)$, and $O(\mu_6)$ bridging atoms, connecting 2, 3, and 6 vanadium atoms, respectively. Table S2 contains V–O and *M*–O bond lengths and bond valences/bond valence sums (BVS) calculated using the following equation [44,45]:

$$s = \exp\left(\frac{R_0 - R}{B}\right) \quad (5)$$

where R is bond length and R_0 and B are empirical parameters for given bond type, to confirm protonation state of the decavanadate anion, oxidation number of V, and central atoms of $[M(H_2O)_5(\beta\text{-HAla})]^{2+}$ complex cations. For V^V–O bonds, the values R_0 = 1.803 Å and B = 0.37 were used [46]. The BVS values obtained are in the range of 1.61–1.76 for V = O_T bonds, 1.764–1.893 for V–O(μ_2) bonds, 1.88–1.92 for V–O(μ_3) bonds, and 1.975–1.998 for V–O(μ_6) bonds. A comparison of BVS values obtained for particular bonds also confirms the rigidity of the $[V_{10}O_{28}]^{6-}$ anion, only marginally influenced by adjacent molecules. For

protonated O atoms, expected BVS values are $\Sigma s < 1.5$; thus, in all prepared compounds, the presence of an unprotonated $[V_{10}O_{28}]^{6-}$ anion was confirmed. BVS values for all V atoms are in the range of 5.02–5.11, confirming oxidation state V(V).

For the BVS calculations for central atoms *M* in $[M(H_2O)_5(\beta\text{-HAla})]^{2+}$ cations, the following values of the bond parameters were used: R_0 = 1.685 Å and B = 0.37 for Co^{2+} in **1** [47], R_0 = 1.675 Å and B = 0.37 for Ni^{2+} in **2** [45], R_0 = 1.904 Å and B = 0.37 for Cd^{2+} in **3** [46], R_0 = 1.704 Å and B = 0.37 for Zn^{2+} in **4** [46], and R_0 = 1.762 Å and B = 0.4 for Mn^{2+} in **5** [48]. In all $[M(H_2O)_5(\beta\text{-HAla})]^{2+}$ cations in the compounds **1**–**5**, oxidation state II for the central atom was confirmed.

All the molecules present in both dihydrates and tetrahydrates are involved in the creation of an extensive hydrogen bonding network (Table S3). Most of these interactions are medium hydrogen bonds with bond distances *d*(H. . .A) between 1.5 to 2.2 Å and bond angles belonging to the range 130–180° after normalisation to neutron distances [49].

The values of average *M*–O distances $\bar{d}$(*M*–O) in $[M(H_2O)_5(\beta\text{-HAla})]^{2+}$ complex cations of the compounds **1**–**5** (Table 1) are in good agreement with the values of the crystal radii for $r(Co^{2+}$ hs) = 85.5 pm, $r(Ni^{2+})$ = 83 pm, $r(Cd^{2+})$ = 109 pm, $r(Zn^{2+})$ = 88 pm, $r(Mn^{2+}$ hs) = 97 pm, and $r(O^{2-})$ = 121 pm, respectively; crystal radii corresponding with low spin states are significantly smaller ($r(Co^{2+}$ ls) = 79 pm, $r(Mn^{2+}$ ls) = 81 pm) [50]. The M–O_{water} distances are in the range 2.070(2)–2.1195(19) Å for **1**, 2.038(2)–2.0729(19) Å for **2**, 2.232(3)–2.327(3) Å for **3**, 2.0665(11)–2.1152(10) Å for **4,** and 2.1369(19)–2.2197(18) for **5**. The M–$O_{\beta\text{-HAla}}$ distances *d*(*M*–O91) (Table S2) are in the range 2.0614(18)–2.200(3) Å in the order of increasing crystal radii. Octahedral distortion parameters in $[M(H_2O)_5(\beta\text{-HAla})]^{2+}$ complex cations (Table 1) also show significant differences between particular values for tetrahydrates and for dihydrates.

Table 1. Average *M*–O distances, octahedral distortion parameters, and octahedron volumes in $[M(H_2O)_5(\beta\text{-HAla})]^{2+}$ complex cations of the compounds **1**–**5**.

Compound	$\bar{d}$(*M*–O) [Å]	ζ	Δ	Σ	Θ	*V* [Å^3]
1	2.090(15)	0.065267	5.1×10^{-5}	21.9313	51.4217	12.14
2	2.055(11)	0.050418	2.7×10^{-5}	23.2468	50.2841	11.54
3	2.26(4)	0.195609	3.10×10^{-4}	53.3874	144.5566	15.30
4	2.090(15)	0.064040	4.8×10^{-5}	28.7336	66.9865	12.14
5	2.17(4)	0.198905	3.38×10^{-4}	43.3304	113.7109	13.47

The zwitterionic form of β-alanine is characterised by the formation of an intramolecular salt bridge between the ammonium group and the carboxylic group, forming a six-membered S(6) ring [51,52]. In tetrahydrates (Figure 3a), smaller Co^{2+}, Ni^{2+}, and Zn^{2+} ions prefer the coordination of the less bulky oxygen atom of the carboxylate group not involved in the intramolecular hydrogen bond, while larger Mn^{2+} and Cd^{2+} cations in dihydrates (Figure 3b) prefer the coordination of the oxygen atom involved in the formation of the intramolecular hydrogen bond. This different behaviour influences not only the strength of the intermolecular hydrogen bond in β-alanine but also the entire hydrogen bond network. As a result, the $[M(H_2O)_5(\beta\text{-HAla})]^{2+}$ cation in tetrahydrates contains two intramolecular hydrogen bonds, i.e., the above-mentioned salt bridge N1–H1. . .O92 between $-NH_3^+$ hydrogen and non-coordinated carboxylate oxygen, and O55–H55B. . .O92 hydrogen bond between coordinated water molecules and the same non-coordinated carboxylate oxygen, thus forming another S(6) supramolecular ring. In dihydrates, the $[M(H_2O)_5(\beta\text{-HAla})]^{2+}$ cation contains one three-centred chelated intramolecular hydrogen bond, i.e., N1–H1B. . .O53 and N1–H1B. . .O91, where H1B belongs to the $-NH_3^+$ group, O53 to the coordinated water molecule, and O91 carboxylate oxygen coordinated to the metal atom. Alongside the intramolecular S(6) ring formed by β-alanine, the S(4) ring involving the coordinated oxygen atom of the carboxylate group, the hydrogen atom of the ammonium group, and the oxygen atom of the coordinated water molecule is formed.

These changes are also reflected as a change in corresponding torsion angles (Table 2) and in the presence of different numbers of cocrystallised water molecules in both crystal forms.

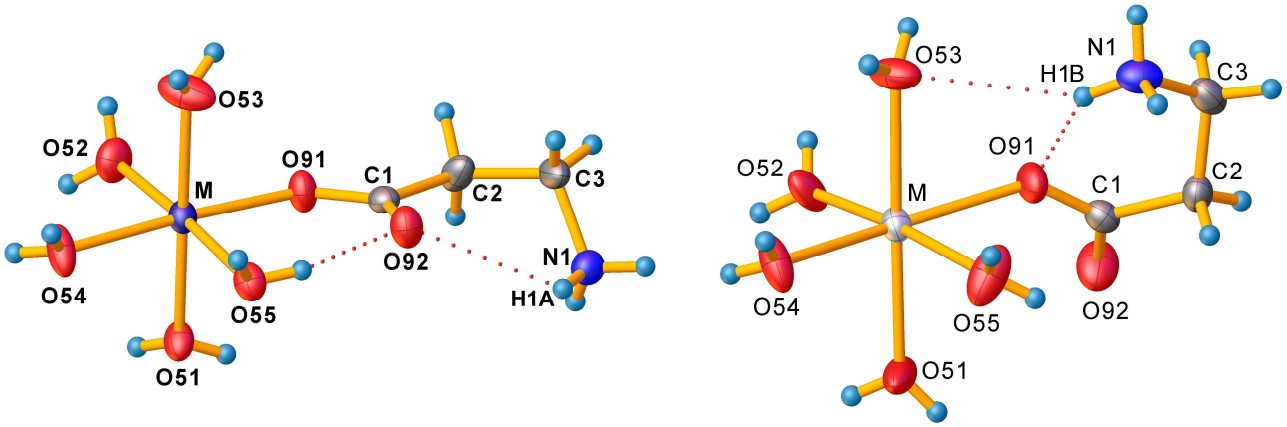

Figure 3. A detailed view of $[M(H_2O)_5(\beta\text{-HAla})]^{2+}$ geometry and intramolecular hydrogen bonds (**a**) in tetrahydrates and (**b**) in dihydrates. Displacement ellipsoids are drawn at 50% probability level.

Table 2. Selected torsion angles in $[M(H_2O)_5(\beta\text{-HAla})]^{2+}$ complex cations of the compounds **1**–**5**.

	1	**2**	**3**	**4**	**5**
M–O91–C1–O92	3.8(4)	0.8(4)	51.7(7)	4.3(2)	59.8(4)
M–O91–C1–C2	−176.41(18)	−179.03(17)	−128.4(4)	−175.70(9)	−119.9(3)
O91–C1–C2–C3	174.9(2)	173.3(2)	−36.8(5)	174.61(12)	−39.3(3)
O92–C1–C2–C3	−5.3(4)	−6.5(4)	143.1(4)	−5.41(18)	141.0(2)
C1–C2–C3–N1	70.5(3)	71.4(3)	59.0(5)	70.03(16)	60.9(3)

3.2. Molar Susceptibility Determination of $[M(H_2O)_5(\beta\text{-HAla})]^{2+}$ Ions in Solution by Paramagnetic ^{1}H-NMR

To determine the spin state of paramagnetic central atoms in the $[M(H_2O)_5(\beta\text{-HAla})]^{2+}$ (M = Co^{II}, Ni^{II}, Mn^{II}) complex cations, molar susceptibilities of the complex cations in the solutions of **1**, **2**, and **5** were determined based on the paramagnetic shift of the ^{1}H-NMR signal of the *t-Bu* group in the paramagnetic solution against the diamagnetic reference (3% *v*/*v* *t-Bu*OH solution in D_2O). For the assessment of diamagnetic contribution, the ^{1}H-NMR chemical shifts of the signal belonging to the *t-Bu* group in the solution of **4** and in a blank sample containing *t-Bu*OH in D_2O were also recorded (Figure 4).

At the concentrations given, there was no significant diamagnetic contribution χ_d from the ligands and other ions in the solution based on a comparison of **4** and blank *t-Bu*OH ^{1}H-NMR spectra, thus μ_{eff} values were calculated directly from χ_m values (Table 3).

Table 3. Experimental data, molar magnetic susceptibilities, and effective magnetic moments of the $[M(H_2O)_5(\beta\text{-HAla})]^{2+}$ complex cations in the compounds **1**, **2,** and **5**.

Compound	**Δ*f* [Hz]**	***c* [mmol.L^{-1}]**	***T* [K]**	**χ_m [cm^{3}mol^{-1}]**	**μ_{eff} [μ_B]**
1	67.576	4.011	302.35	0.010052	4.95
2	30.2619	4.004	302.25	0.004509	3.32
5	95.534	4.000	300.85	0.014235	5.88

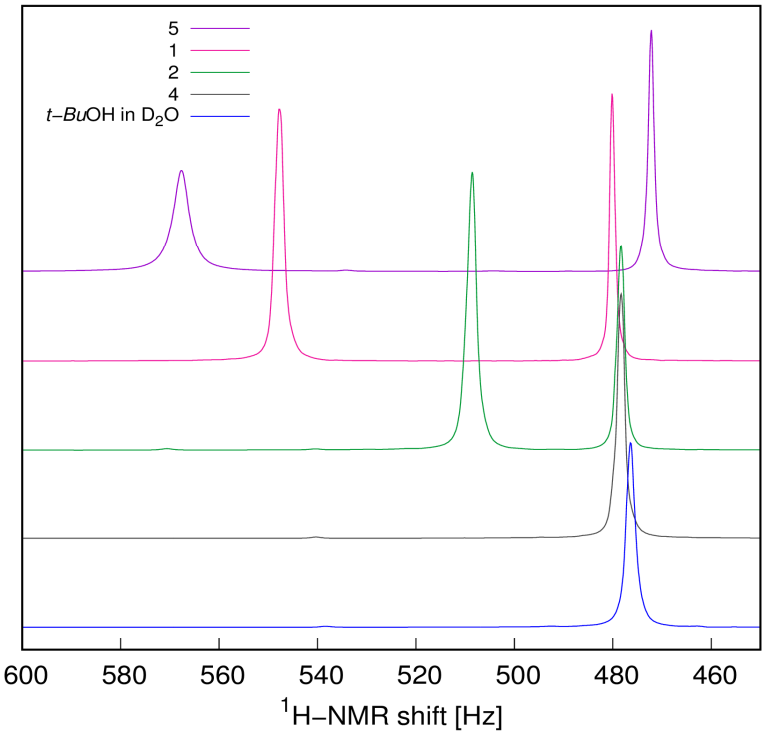

Figure 4. Paramagnetic shifts of the *t-Bu* ^{1}H-NMR signal in the solutions of the compounds **1**, **2**, **4,** and **5** and a blank sample against the reference solution of *t-Bu*OH in D_2O.

The results are in good agreement with the calculated μ_{cal} values by using Equation (4) for three unpaired electrons of Co^{2+}(hs) in **1**, two unpaired electrons of Ni^{2+} in **2,** and five unpaired electrons of Mn^{2+}(hs) in **5**. These findings agree with the assignment of spin states based on average $\overline{d}$(*M*–O) distances.

3.3. Vibrational Spectroscopy

The FT-IR (Figure 5a) and FT-Raman (Figure 5b) spectra of crystalline **1**–**5** are quite similar because of the same chemical components present. The FT-IR and FT-Raman spectra of the individual compounds are mutually compared on Figure S1a–e. The assignments of the bands are summarised in Table S4 [7,21,53].

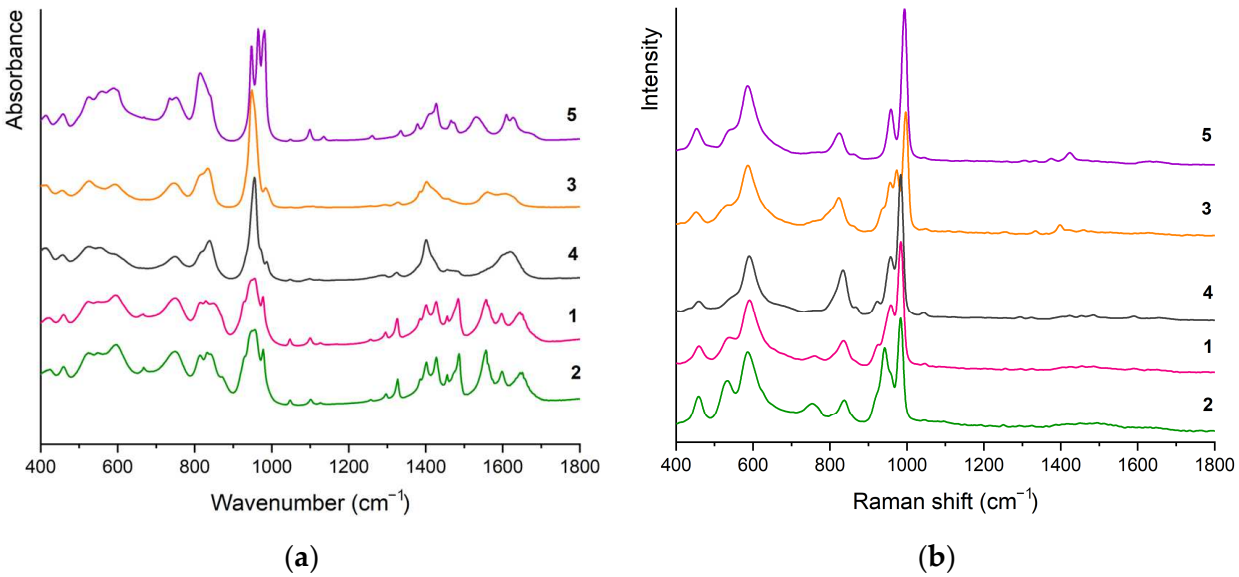

Figure 5. Stacked FT-IR (**a**) and FT-Raman (**b**) spectra of the compounds **1**–**5**.

The common features of decavanadate IR spectra involve the bands with highest intensity in the range 920–1000 cm^{-1} corresponding to valence vibrations of terminal V=O bonds and two broad series of bands related to asymmetric and symmetric bridging O–V_2 vibration modes in the range of 843–748 cm^{-1} (ν_{as}, IR)/866–823 cm^{-1} (ν_{as}, Raman) and 596–524 cm^{-1} (ν_s, IR)/591–533 cm^{-1} (ν_s, Raman), respectively.

The assignment of the bands corresponding to $\delta_d(NH_3^+)$, $\delta_d(NH_4^+)$, and both ν_s and $\nu_{as}(COO^-)$, is based on a comparison of partially deuterated samples [21].

To distinguish between binding modes of carboxylate group in complexes, it is possible to use the differences between frequencies of asymmetric and symmetric stretching vibrations, $\Delta = \nu_{as}(COO^-)—\nu_s(COO^-)$. Carboxylato complexes exhibiting Δ values that are significantly greater than ionic values, typically with $\Delta \geq 200$ cm^{-1} (cf. 164 and 184 cm^{-1} for zwitterionic β-HAla [53]), have usually unidentate coordination [54]. The Δ values of studied compounds (Δ = 230 for **1**, **2,** and **3**; Δ = 233 for **4;** and Δ = 199 for **5**) are typical for monodentate mode of carboxylate group bonding, thus confirming the results of X-ray structure analysis.

The presence of water molecules is confirmed by the bands in the region 3484–3380 cm^{-1}. These bands usually appear in the 3600–3400 cm^{-1} range, and their shift towards lower wavenumbers is caused by the occurrence of O–H. . .O hydrogen bonds.

4. Conclusions

We prepared $(NH_4)_2[Co(H_2O)_5(\beta\text{-HAla})]_2[V_{10}O_{28}]\cdot 4H_2O$, $(NH_4)_2[Ni(H_2O)_5(\beta\text{-HAla})]_2[V_{10}O_{28}]\cdot 4H_2O$, and $(NH_4)_2[Cd(H_2O)_5(\beta\text{-HAla})]_2[V_{10}O_{28}]\cdot 2H_2O$ by synthesising them in a mildly acidic aqueous solution, which, in comparison with hydrothermal direct synthesis from metallic powder and V_2O_5, prevented partial reduction of V(V) to V(IV) during the preparation of $(NH_4)_2[Co(H_2O)_5(\beta\text{-HAla})]_2[V_{10}O_{28}]\cdot 4H_2O$. The prepared compounds were characterised by X-ray structure analysis and vibration spectroscopy. The FT-IR and FT-Raman spectra confirmed the presence of the $[V_{10}O_{28}]^{6-}$ anion and monodentate coordination mode of β-HAla in complex cation in accordance with crystallographic findings. To confirm the spin state of central atoms in $[M(H_2O)_5(\beta\text{-HAla})]^{2+}$ cations, including previously prepared $(NH_4)_2[Mn(H_2O)_5(\beta\text{-HAla})]_2[V_{10}O_{28}]\cdot 2H_2O$, the Evans method was used to confirm the assignment of spin states based on crystallographic data. The increasing crystal radius of central atoms and their different preferences for donor atoms resulting in rebuilding of the hydrogen bonding network is the main cause of the existence of two different crystallohydrate forms.

Supplementary Materials: The following supporting information can be downloaded at: https://www.mdpi.com/article/10.3390/cryst14080685/s1. Table S1: Crystallographic data for the compounds **1**–**5**; Table S2: Selected bond lengths, bond valences and bond valence sums in the compounds **1**–**5**; Table S3: Hydrogen bonds in the structures of **1**–**5**; Figure S1a: A comparison of IR and Raman spectra of **1**; Figure S1b: A comparison of IR and Raman spectra of **2**; Figure S1c: A comparison of IR and Raman spectra of **3**; Figure S1d: A comparison of IR and Raman spectra of **4**; Figure S1e: A comparison of IR and Raman spectra of **5**. Table S4: Assignments of the IR and Raman absorption bands for compounds **1**–**5** [7,21,53].

Author Contributions: Conceptualisation, L.B. and E.R.; methodology, J.C. and E.R.; validation, J.C. and E.R.; formal analysis, Y.R.P. and E.R.; investigation, L.B., J.C., Y.R.P. and E.R.; resources, L.B.; data curation, E.R.; writing—original draft preparation, E.R. and Y.R.P.; writing—review and editing, E.R. and J.C.; visualisation, E.R. and J.C.; project administration, E.R. and Y.R.P.; funding acquisition, Y.R.P. and E.R. All authors have read and agreed to the published version of the manuscript.

Funding: This work was supported by the Grant of Comenius University no. UK/3049/2024, Scientific Grant Agency of the Ministry of Education of the Slovak Republic and of Slovak Academy of Sciences VEGA 1/0669/22, and Slovak Research and Development Agency under Contract no. APVV-21-0503.

Data Availability Statement: The deposition numbers CCDC 2366040—2366044 contain the supplementary crystallographic data for this article, including structure factors. These data can be obtained free of charge at https://www.ccdc.cam.ac.uk/structures/ (accessed date 23 July 2024). Crystallographic data can also be obtained from the Crystallography Open Database (COD) under COD ID 3000552—3000556.

Acknowledgments: The authors thank Aleksandra Cyganiuk from Nicolaus Copernicus University in Toruń (Poland) for the Raman spectra measurements.

Conflicts of Interest: The authors declare no conflicts of interest.

References

1. Hayashi, Y. Hetero and Lacunary Polyoxovanadate Chemistry: Synthesis, Reactivity and Structural Aspects. *Coord. Chem. Rev.* **2011**, *255*, 2270–2280. [CrossRef]
2. Kempf, J.Y.; Rohmer, M.M.; Poblet, J.M.; Bo, C.; Benard, M. Relative basicities of the oxygen sites in $[V_{10}O_{28}]^{6-}$. An analysis of the ab initio determined distributions of the electrostatic potential and of the Laplacian of charge density. *J. Am. Chem. Soc.* **1992**, *114*, 1136–1146. [CrossRef]
3. Day, V.W.; Klemperer, W.G.; Maltbie, D.J. Where are the protons in $H_3V_{10}O_{28}^{3-}$? *J. Am. Chem. Soc.* **1987**, *109*, 2991–3002. [CrossRef]
4. Biagioli, M.; Strinna-Erre, L.; Micera, G.; Panzanelli, A.; Zema, M. Tetrahydrogendecavanadate(V) and Its Binding to Glycylglycine. *Inorg. Chem. Commun.* **1999**, *2*, 214–217. [CrossRef]
5. Rakovský, E.; Joniaková, D.; Gyepes, R.; Schwendt, P.; Mička, Z. Synthesis and Crystal Structure of $[CuCl(phen)_2]_3H_3V_{10}O_{28}\cdot 7H_2O$. *Cryst. Res. Technol.* **2005**, *40*, 719–722. [CrossRef]
6. Kaziev, G.Z.; Oreshkina, A.V.; Stepnova, A.F.; Holguin Quinones, S.; Stash, A.I.; Morales Sanchez, L.A. Synthesis and Study of the Physicochemical Properties of Ammonium Hydrogen Hexaaquacobaltate(III) Isopolyvanadate $[(NH_4)_2][Co(H_2O)_6]\cdot H[V_{10}O_{28}]\cdot 8H_2O$. *Russ. J. Coord. Chem.* **2011**, *37*, 766–771. [CrossRef]
7. Sánchez-Lara, E.; Pérez-Benítez, A.; Treviño, S.; Mendoza, A.; Meléndez, F.J.; Sánchez-Mora, E.; Bernès, S.; González-Vergara, E. Synthesis and 3D Network Architecture of 1- and 16-Hydrated Salts of 4-Dimethylaminopyridinium Decavanadate, $(DMAPH)_6[V_{10}O_{28}]\cdot nH_2O$. *Crystals* **2016**, *6*, 65. [CrossRef]
8. Lv, Y.-K.; Jiang, Z.-G.; Gan, L.-H.; Liu, M.-X.; Feng, Y.-L. Three Novel Organic-Inorganic Hybrid Materials Based on Decaoxovanadates Obtained from a New Liquid Phase Reaction. *CrystEngComm* **2012**, *14*, 314–322. [CrossRef]
9. Ferreira da Silva, J.L.; Fátima Minas da Piedade, M.; Teresa Duarte, M. Decavanadates: A Building-Block for Supramolecular Assemblies. *Inorganica Chim. Acta* **2003**, *356*, 222–242. [CrossRef]
10. Crans, D.C.; Smee, J.J.; Gaidamauskas, E.; Yang, L. The Chemistry and Biochemistry of Vanadium and the Biological Activities Exerted by Vanadium Compounds. *Chem. Rev.* **2004**, *104*, 849–902. [CrossRef]
11. Aureliano, M.; Gumerova, N.I.; Sciortino, G.; Garribba, E.; Rompel, A.; Crans, D.C. Polyoxovanadates with Emerging Biomedical Activities. *Coord. Chem. Rev.* **2021**, *447*, 214143. [CrossRef]
12. Aureliano, M.; Gumerova, N.I.; Sciortino, G.; Garribba, E.; McLauchlan, C.C.; Rompel, A.; Crans, D.C. Polyoxidovanadates' Interactions with Proteins: An Overview. *Coord. Chem. Rev.* **2022**, *454*, 214344. [CrossRef]
13. Samart, N.; Saeger, J.; Haller, K.J.; Aureliano, M.; Crans, D.C. Interaction of Decavanadate With Interfaces and Biological Model Membrane Systems: Characterization of Soft Oxometalate Systems. *J. Mol. Eng. Mater.* **2014**, *02*, 1440007. [CrossRef]
14. Aureliano, M.; Gândara, R.M.C. Decavanadate Effects in Biological Systems. *J. Inorg. Biochem.* **2005**, *99*, 979–985. [CrossRef] [PubMed]
15. Buvailo, H.I.; Pavliuk, M.V.; Makhankova, V.G.; Kokozay, V.N.; Bon, V.; Mijangos, E.; Shylin, S.I.; Jezierska, J. Facile One-Pot Synthesis of Hybrid Compounds Based on Decavanadate Showing Water Oxidation Activity. *Inorg. Chem. Commun.* **2020**, *119*, 108111. [CrossRef]
16. Huang, X.; Gu, X.; Qi, Y.; Zhang, Y.; Shen, G.; Yang, B.; Duan, W.; Gong, S.; Xue, Z.; Chen, Y. Decavanadate-Based Transition Metal Hybrids as Bifunctional Catalysts for Sulfide Oxidation and C—C Bond Construction. *Chin. J. Chem.* **2021**, *39*, 2495–2503. [CrossRef]
17. Cao, J.-P.; Shen, F.-C.; Luo, X.-M.; Cui, C.-H.; Lan, Y.-Q.; Xu, Y. Proton Conductivity Resulting from Different Triazole-Based Ligands in Two New Bifunctional Decavanadates. *RSC Adv.* **2018**, *8*, 18560–18566. [CrossRef] [PubMed]
18. Kang, R.; Cao, J.; Han, Y.; Hong, Y.; Yang, M.; Xu, Y. Three New Ln-Decavanadates Materials: Synthesis, Structure, and Photoluminescent Sensing for Detection of Zn^{2+} and Co^{2+}. *Zeitschrift Anorg. Allg. Chem.* **2020**, *646*, 1315–1323. [CrossRef]
19. Kumar, D.; Tomar, A.K.; Singal, S.; Singh, G.; Sharma, R.K. Ammonium Decavanadate Nanodots/Reduced Graphene Oxide Nanoribbon as "Inorganic-Organic" Hybrid Electrode for High Potential Aqueous Symmetric Supercapacitors. *J. Power Sources* **2020**, *462*, 228173. [CrossRef]
20. Kumar, D.; Tomar, A.K.; Singh, G.; Sharma, R.K. Interlayer Gap Widened 2D α-$Co(OH)_2$ Nanoplates with Decavanadate Anion for High Potential Aqueous Supercapacitor. *Electrochim. Acta* **2020**, *363*, 137238. [CrossRef]
21. Klištincová, L.; Rakovský, E.; Schwendt, P. Decavanadates with Complex Cations: Synthesis and Structure of $(NH_4)_2[M(H_2O)_5(NH_3CH_2CH_2COO)]_2V_{10}O_{28}\cdot nH_2O$ (*M.* = Zn^{II}, *n* = 4; *M.* = Mn^{II}, *n* = 2). *Transit. Met. Chem.* **2010**, *35*, 229–236. [CrossRef]

22. Pavliuk, M.V.; Makhankova, V.G.; Kokozay, V.N.; Omelchenko, I.V.; Jezierska, J.; Thapper, A.; Styring, S. Structural, Magnetic, Thermal and Visible Light-Driven Water Oxidation Studies of Heterometallic Mn/V Complexes. *Polyhedron* **2015**, *88*, 81–89. [CrossRef]
23. Pavliuk, M.V.; Mijangos, E.; Makhankova, V.G.; Kokozay, V.N.; Pullen, S.; Liu, J.; Zhu, J.; Styring, S.; Thapper, A. Homogeneous Cobalt/Vanadium Complexes as Precursors for Functionalized Mixed Oxides in Visible-Light-Driven Water Oxidation. *ChemSusChem* **2016**, *9*, 2957–2966. [CrossRef] [PubMed]
24. Rigaku Oxford Diffraction. *CrysAlisPro Software System, Version 1.171.43.128a*; Rigaku Corporation: Wroclaw, Poland, 2024.
25. Sheldrick, G.M. SHELXT—Integrated Space-Group and Crystal-Structure Determination. *Acta Crystallogr. Sect. A Found. Adv.* **2015**, *71*, 3–8. [CrossRef]
26. Sheldrick, G.M. Crystal Structure Refinement with SHELXL. *Acta Crystallogr. Sect. C Struct. Chem.* **2015**, *71*, 3–8. [CrossRef] [PubMed]
27. Bourhis, L.J.; Dolomanov, O.V.; Gildea, R.J.; Howard, J.A.K.; Puschmann, H. The Anatomy of a Comprehensive Constrained, Restrained Refinement Program for the Modern Computing Environment—Olex2 Dissected. *Acta Crystallogr. Sect. A Found. Adv.* **2015**, *71*, 59–75. [CrossRef] [PubMed]
28. Nardelli, M. PARST 95—An Update to PARST: A System of Fortran Routines for Calculating Molecular Structure Parameters from the Results of Crystal Structure Analyses. *J. Appl. Crystallogr.* **1995**, *28*, 659. [CrossRef]
29. Brandenburg, K. *Diamond. Release 3.2k*; Crystal Impact GbR: Bonn, Germany, 2014.
30. Buron-Le Cointe, M.; Hébert, J.; Baldé, C.; Moisan, N.; Toupet, L.; Guionneau, P.; Létard, J.F.; Freysz, E.; Cailleau, H.; Collet, E. Intermolecular Control of Thermoswitching and Photoswitching Phenomena in Two Spin-Crossover Polymorphs. *Phys. Rev. B Condens. Matter Mater. Phys.* **2012**, *85*, 064114. [CrossRef]
31. Lufaso, M.W.; Woodward, P.M. Jahn-Teller Distortions, Cation Ordering and Octahedral Tilting in Perovskites. *Acta Crystallogr. Sect. B Struct. Sci.* **2004**, *60*, 10–20. [CrossRef]
32. Marchivie, M.; Guionneau, P.; Létard, J.F.; Chasseau, D. Photo-Induced Spin-Transition: The Role of the Iron(II) Environment Distortion. *Acta Crystallogr. Sect. B Struct. Sci.* **2005**, *61*, 25–28. [CrossRef]
33. McCusker, J.K.; Rheingold, A.L.; Hendrickson, D.N. Variable-Temperature Studies of Laser-Initiated $^5T_2 \rightarrow {}^1A_1$ Intersystem Crossing in Spin-Crossover Complexes: Empirical Correlations between Activation Parameters and Ligand Structure in a Series of Polypyridyl Ferrous Complexes. *Inorg. Chem.* **1996**, *35*, 2100–2112. [CrossRef]
34. Ketkaew, R.; Tantirungrotechai, Y.; Harding, P.; Chastanet, G.; Guionneau, P.; Marchivie, M.; Harding, D.J. OctaDist: A Tool for Calculating Distortion Parameters in Spin Crossover and Coordination Complexes. *J. Chem. Soc. Dalt. Trans.* **2021**, *50*, 1086–1096. [CrossRef] [PubMed]
35. Jeffrey, G.A.; Lewis, L. Cooperative Aspects of Hydrogen Bonding in Carbohydrates. *Carbohydr. Res.* **1978**, *60*, 179–182. [CrossRef]
36. Taylor, R.; Kennard, O. Comparison of X-ray and Neutron Diffraction Results for the N-H $\cdots$O=C Hydrogen Bond. *Acta Crystallogr. Sect. B* **1983**, *39*, 133–138. [CrossRef]
37. Evans, D.F. The Determination of the Paramagnetic Susceptibility of Substances in Solution by Nuclear Magnetic Resonance. *J. Chem. Soc.* **1959**, 2003–2005. [CrossRef]
38. Evans, D.F.; Fazakerley, G.V.; Phillips, R.F. Organometallic Compounds of Bivalent Europium, Ytterbium, and Samarium. *J. Chem. Soc. A Inorg. Phys. Theor. Chem.* **1971**, 1931–1934. [CrossRef]
39. Schubert, E.M. Utilizing the Evans Method with a Superconducting NMR Spectrometer in the Undergraduate Laboratory. *J. Chem. Educ.* **1992**, *69*, 62. [CrossRef]
40. Bain, G.A.; Berry, J.F. Diamagnetic Corrections and Pascal's Constants. *J. Chem. Educ.* **2008**, *85*, 532–536. [CrossRef]
41. Mugiraneza, S.; Hallas, A.M. Tutorial: A Beginner's Guide to Interpreting Magnetic Susceptibility Data with the Curie-Weiss Law. *Commun. Phys.* **2022**, *5*, 95. [CrossRef]
42. Rakovský, E.; Krivosudský, L. Tetrakis(2,6-Dimethylpyridinium) Dihydrogen Decavanadate Dihydrate. *Acta Crystallogr. Sect. E Struct. Rep. Online* **2014**, *70*, m225–m226. [CrossRef]
43. Cooper, R.I.; Thompson, A.L.; Watkin, D.J. CRYSTALS Enhancements: Dealing with Hydrogen Atoms in Refinement. *J. Appl. Crystallogr.* **2010**, *43*, 1100–1107. [CrossRef]
44. Brown, I.D. *The Chemical bond in Inorganic Chemistry*; IUCr Monographs on Crystallography; Oxford University Press: New York, NY, USA, 2002; Volume 12.
45. (IUCr) Bond Valence Parameters. Available online: https://www.iucr.org/__data/assets/file/0011/150779/bvparm2020.cif (accessed on 23 July 2024).
46. Brown, I.D.; Altermatt, D. Bond-Valence Parameters Obtained from a Systematic Analysis of the Inorganic Crystal Structure Database. *Acta Crystallogr. Sect. B Struct. Sci.* **1985**, *41*, 244–247. [CrossRef]
47. Wood, R.M.; Palenik, G.J. Bond Valence Sums in Coordination Chemistry. A Simple Method for Calculating the Oxidation State of Cobalt in Complexes Containing Only Co−O Bonds. *Inorg. Chem.* **1998**, *37*, 4149–4151. [CrossRef] [PubMed]
48. Urusov, V.S. Problem of Optimization of Bond Valence Model Parameters (as Exemplified by Managanese in Different Oxidation States). *Dokl. Phys. Chem.* **2006**, *408*, 152–155. [CrossRef]
49. Jeffrey, G.A. *An Introduction to Hydrogen Bonding*, 1st ed.; Oxford University Press: New York, NY, USA, 1997; p. 12.
50. Shannon, R.D. Revised Effective Ionic Radii and Systematic Studies of Interatomie Distances in Halides and Chaleogenides. *Acta Crystallogr. Sect. A* **1976**, *32*, 751–767. [CrossRef]

51. Etter, M.C.; MacDonald, J.C.; Bernstein, J. Graph-Set Analysis of Hydrogen-Bond Patterns in Organic Crystals. *Acta Crystallogr. Sect. B Struct. Sci.* **1990**, *46*, 256–262. [CrossRef] [PubMed]
52. Bernstein, J.; Davis, R.E.; Shimoni, L.; Chang, N.-L. Patterns in Hydrogen Bonding: Functionality and Graph Set Analysis in Crystals. *Angew. Chemie Int. Ed. Engl.* **1995**, *34*, 1555–1573. [CrossRef]
53. Berezhinsky, L.I.; Dovbeshko, G.I.; Lisitsa, M.P.; Litvinov, G.S. Vibrational Spectra of Crystalline β-Alanine. *Spectrochim. Acta Part A Mol. Biomol. Spectrosc.* **1998**, *54*, 349–358. [CrossRef]
54. Deacon, G.B.; Phillips, R.J. Relationships between the carbon-oxygen stretching frequencies of carboxylato complexes and the type of carboxylate coordination. *Coord. Chem. Rev.* **1980**, *33*, 227–250. [CrossRef]

Disclaimer/Publisher's Note: The statements, opinions and data contained in all publications are solely those of the individual author(s) and contributor(s) and not of MDPI and/or the editor(s). MDPI and/or the editor(s) disclaim responsibility for any injury to people or property resulting from any ideas, methods, instructions or products referred to in the content.